Lattice thermal conductivity of single-walled carbon nanotubes: Beyond the relaxation time approximation and phonon-phonon scattering selection rules

L. Lindsay and D. A. Broido
Department of Physics, Boston College, Chestnut Hill, Massachusetts 02467, USA

Natalio Mingo
CEA-Grenoble, 17 Rue des Martyrs, Grenoble 38000, France
and Department of Electrical Engineering, University of California, Santa Cruz, California 95064, USA
(Received 13 May 2009; revised manuscript received 13 August 2009; published 11 September 2009)

We present a theoretical description of phonon thermal transport and intrinsic lattice thermal conductivity in single-walled carbon nanotubes (SWCNTs). An exact solution of the phonon Boltzmann equation is implemented using an efficient scheme that allows consideration of SWCNTs with a wide range of radii and chiralities. Our approach combines for the first time calculations of the full spectrum of anharmonic three-phonon scattering processes in SWCNTs with use of the correct selection rules that severely restrict the phase space of this scattering. In particular, we demonstrate that if only the acoustic phonon branches are considered, no umklapp scattering can occur: *scattering of acoustic phonons by optic phonons is required to produce thermal resistance in SWCNTs*. We also show that the commonly used relaxation time approximation gives a particularly poor description of thermal transport in SWCNTs because of the unusually weak phonon-phonon umklapp scattering in these systems.

DOI: 10.1103/PhysRevB.80.125407 PACS number(s): 68.65.−k, 65.80.+n, 63.22.−m, 63.20.kg

I. INTRODUCTION

In crystalline semiconductors and insulators intrinsic thermal resistance arises from phonon-phonon scattering, which occurs because of the anharmonicity of the interatomic potential.[1] The resistive umklapp scattering processes are typically strong around room temperature where they dominate the behavior of the intrinsic lattice thermal conductivity. Carbon based materials such as diamond, graphite, graphene, and carbon nanotubes are uniquely different. In these materials, the strong bond stiffness and light atomic mass produce extremely high phonon frequencies and acoustic velocities. As a result, the phase space available for umklapp scattering is unusually small.[2] These factors facilitate large amounts of heat being carried by acoustic phonon modes and contribute to making these carbon-based structures have the highest thermal conductivities of any known materials.[3–7] These materials are therefore of great scientific interest as well as attractive candidates for passive thermal management applications.

In this work, we focus on the unusual phonon thermal transport properties of single-walled carbon nanotubes (SWCNTs), which are connected to their unique phonon dispersions and to phonon-phonon scattering. Many previous theoretical investigations of lattice thermal conductivity in SWCNTs have been performed. However, widely varying results have been obtained,[8–13] and qualitative disagreements have arisen regarding whether the thermal conductivity diverges with nanotube length. Theoretical investigations have been divided into molecular dynamics (MD) approaches[8,9] and Boltzmann transport equation (BTE) approaches.[10–13] As our interest is in explicit examination of phonon-phonon scattering, we employ here the latter approach.

Several previous calculations of the phonon thermal conductivity of SWCNTs have been performed using phonon BTE approaches.[10–13] Most of these[10–12] have employed the single-mode relaxation time approximation (RTA) whereby each phonon mode is characterized by a single relaxation time independent of all other modes. These RTA approaches have included umklapp scattering, but they have omitted normal three-phonon scattering processes. They have also used model interatomic potentials that do not satisfy the correct rotational symmetry constraints.[14] Also, previous BTE approaches[10–13] have not used the correct selection rule for three-phonon umklapp scattering. This selection rule is revealed through the full calculations of the three-phonon matrix elements performed here, but was masked in previous work because these employed a commonly used long-wavelength approximation (LWA) for the three-phonon scattering rates derived for bulk materials at low temperatures.[15]

In this work, we use an exact solution of the linearized phonon BTE to calculate the intrinsic thermal conductivity of SWCNTs as a function of their length. We employ an interatomic potential that correctly represents the symmetries of the SWCNTs. Instead of the commonly used LWA, we employ full quantum mechanical calculations of both normal and umklapp three-phonon scattering processes, and we include phonon-phonon scattering between all acoustic and optic modes. We employ for the first time the correct selection rules for three-phonon umklapp scattering. These selection rules dictate that the heat carrying acoustic modes can only undergo resistive umklapp scattering with optic modes. Thus, *three-phonon scattering between only acoustic modes can provide no thermal resistance*, a point that has been missed in previous work.[10–13] Furthermore, the strongly restricted phase space for umklapp scattering causes the thermal conductivity of SWCNTs to be considerably higher than that obtained in the RTA. The above points highlight the importance of employing a rigorous approach to examine phonon thermal transport in SWCNTs.

Section II presents the theoretical approach used to calculate the thermal conductivity of SWCNTS. In Sec. III, results are presented and discussed. Sec. IV presents a summary and conclusions.

II. THEORY

We will consider here achiral [$(n,0)$ for zigzag and (n,n) for armchair] SWCNTs. The generalization to chiral SWCNTs is straightforward and will be discussed briefly later. We describe the nanotube starting with a two-atom unit cell. The entire SWCNT can then be generated using linear combinations of two screw operations on this unit cell.[16] Translational[17] and rotational[16,18,19] boundary conditions allow a phonon to be specified by the three quantum numbers (q, l, j), where q is the dimensionless wave number associated with the translational periodicity along the tube axis, $-\pi < q \leq \pi$, the angular quantum number, l, is connected to the rotational symmetry and takes on the integral values $l=0, \pm 1, \ldots +n$, and j is one of six phonon branches for a given two-dimensional wave vector, $\mathbf{q}=(q,l)$. We will consider SWCNTs of sufficient length that q is taken to be continuous. The phonon frequencies, ω_λ, and eigenvectors, $\hat{e}^\lambda$, are obtained by diagonalizing the corresponding 6×6 dynamical matrices constructed for each $\mathbf{q}$,[20] where λ is a shorthand for the triplet of quantum numbers specifying a phonon mode: $\lambda=(q,l,j)$. For $(n,0)$ or (n,n) nanotubes, the phonon spectrum consists of four "acoustic" branches and $4(3n\text{-}1)$ optic branches. The torsional (T) and longitudinal (L) acoustic branches have linear dispersions $(\omega \propto q)$ at long wavelength and correspond to $(l,j)=(0,1)$ and $(0,2)$, respectively, while two degenerate flexure (F) modes have quadratic dispersions $(\omega \propto q^2)$ at long wavelength and correspond to $(l,j)=(\pm 1,1)$.[14,20]

Calculation of the phonon spectrum and the phonon-phonon scattering rates requires the harmonic and anharmonic interatomic force constants (IFCs). These are obtained using the Tersoff empirical interatomic potential.[21] For each SWCNT considered the potential energy is minimized allowing for atomic relaxation. We note that the translational and rotational symmetry for this defect free structure is preserved. Differentiation of this potential yields the required IFCs. These IFCs must satisfy sum rules connected to the translational and rotational invariance.[14,20,22] Potentials that do not satisfy these rules can lead to physically incorrect results such as flexure modes that have linear instead of quadratic dispersions.[14] For the IFCs used here, we have verified that the above sum rules are indeed satisfied for each SWCNT considered.

The intrinsic lattice thermal conductivity of a SWCNT, κ, is limited only by (a) phonon-phonon scattering and (b) "boundary" scattering connected to its finite length.[23] The SWCNT is taken to be free of impurities and defects. κ can be expressed as[1]

$$\kappa = \frac{1}{V}\sum_\lambda C_\lambda v_\lambda^2 \tau_\lambda, \tag{1}$$

where the mode specific heat is $C_\lambda = k_B(\hbar\omega_\lambda\beta)^2 n_\lambda^0(n_\lambda^0+1)$, $\beta = 1/k_BT$, n_λ^0 is the Bose distribution function, v_λ is the phonon velocity in the mode λ, and τ_λ is the phonon scattering time. We take the nanotube volume, V, to be given by the commonly used expression, $V=A\times L$, where L is the nanotube length, and $A=\pi d\delta$ is the cross-sectional area, with d being the nanotube diameter, and $\delta=3.35$ Å the separation between the carbon planes in graphite.[24] To lowest order, phonon-phonon interactions are described by the scattering of three phonons.[1] The three-phonon scattering rates for "+" and "–" processes, $(q,l)\pm(q',l')\leftrightarrow(q'',l'')$, can be expressed using Fermi's golden rule as

$$W^{(\pm)}_{\lambda\lambda'\lambda''} = \frac{\pi\hbar}{4N_0}\frac{(n_\lambda^0+1)(n_{\lambda'}^0+1/2\pm 1/2)n_{\lambda''}^0}{\omega_\lambda\omega_{\lambda'}\omega_{\lambda''}} \times|\Phi^{(\pm)}_{\lambda\lambda'\lambda''}|^2\delta(\omega_\lambda \pm \omega_{\lambda'} - \omega_{\lambda''}), \tag{2}$$

where N_0 is the number of two-atom unit cells in the nanotube, and the three-phonon matrix element is

$$\Phi^{(\pm)}_{\lambda\lambda'\lambda''} = \delta_{\mathbf{q}\pm\mathbf{q}',\mathbf{q}''+\mathbf{G}}\sum_\kappa\sum_{\ell'\kappa'}\sum_{\ell''\kappa''}\sum_{\alpha\beta\gamma}\Phi_{\alpha\beta\gamma}(0\kappa,\ell'\kappa',\ell''\kappa'') \times e_\alpha^{-\lambda}(0\kappa)e_\beta^{\mp\lambda'}(\ell'\kappa')e_\gamma^{\lambda''}(\ell''\kappa''). \tag{3}$$

In Eq. (3), $\ell\kappa$ locates the κth atom in unit cell $\ell=(\ell_1,\ell_2)$ requiring ℓ_i successive screw operations of type $i=1,2$,[20] $\Phi_{\alpha\beta\gamma}(0\kappa,\ell'\kappa',\ell''\kappa'')$ are the third-order IFCs, and α, β, and γ are cartesian components. The scaled phonon eigenvectors for unit cell $\ell\kappa$ are[20]

$$e_\alpha^\lambda(\ell\kappa) = \frac{1}{\sqrt{M_\kappa}}\sum_\beta S_{\alpha\beta}(\ell)e_{\beta\kappa}^\lambda \exp(i\mathbf{q}\cdot\mathbf{R}_\ell). \tag{4}$$

Here, $e_{\beta\kappa}^\lambda$ is the βth component of the eigenvector connected to the κth atom in the starting unit cell, $S_{\alpha\beta}(\ell)$ is a rotation matrix, and $\mathbf{R}_\ell=[\theta(\ell),z(\ell)]$ is the vector specifying the dimensionless coordinates of cell ℓ.[20] Also, M_κ is the mass of the κth atom, and $\lambda\rightarrow-\lambda$ signifies complex conjugation of the eigenvectors for which $q\rightarrow -q$, and $l\rightarrow -l$. The two-component vector, $\boldsymbol{G}=(G,l_G)$, is composed of the one-dimensional reciprocal lattice vector associated with the translational periodicity, $G=2\pi m$, $m=0,\pm 1,\pm 2,\ldots$, and an integer, l_G, described below.

The delta-function in Eq. (3) enforces momentum selection rules for three-phonon scattering in SWCNTs that are presented in the first two equations below, along with the energy conservation condition required in each three-phonon process from Eq. (2),

$$q \pm q' = q'' + G, \tag{5a}$$

$$l \pm l' = (l'' + l_G)\text{mod } 2n, \tag{5b}$$

$$\omega_\lambda \pm \omega_{\lambda'} = \omega_{\lambda''}. \tag{5c}$$

Here the mod function keeps $l''+l_G$ between $-n+1$ and n. For normal (N) scattering processes, $G=l_G=0$. For umklapp (U) processes, $G\neq 0$ and is chosen so that q'' lies in the first Brillouin zone, and the integer $l_G=\pm n$ for achiral nanotubes. We note that l is not rigorously conserved for umklapp pro-

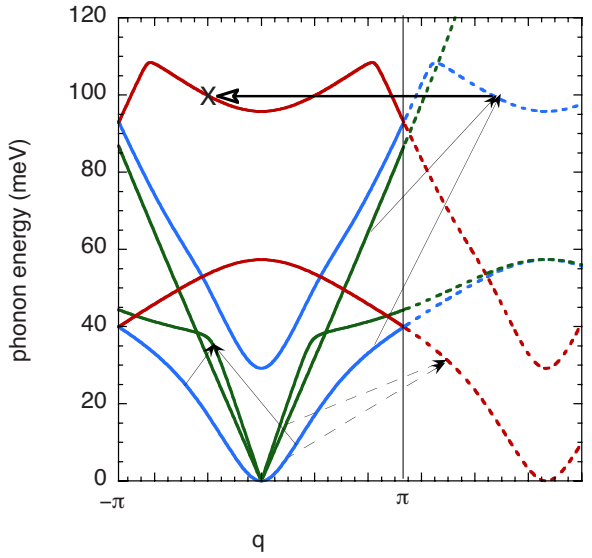

FIG. 1. (Color online) Phonon dispersion for a (10,0) SWCNT showing the lowest two linear acoustic branches (green curves) with $l=0$, the lowest two degenerate flexure branches and optic branches (blue curves) with $l=\pm 1$, and the lowest two optic branches (red curves) with $l=-9$. The portions of the branches inside (outside) the first Brillouin zone are solid (dashed). N and U three-phonon processes are indicated by the thin arrow pairs, with the horizontal arrow showing the projection into the first Brillouin zone. Dashed arrows are for a fictitious U process forbidden by the l selection rule.

cesses because it arises from the isogonal point group, $\mathbf{D}_{2nh}$, which is not a subgroup of the nanotube line group.[25,26] This point has been missed in previous calculations.[10–13]

The conservation conditions, Eq. (5), severely restrict the phase space of N and U three-phonon scattering in SWCNTs. Consider processes where two phonons in F branches (1,1) and $(-1,1)$ decay into a third phonon. According to the l selection rule, Eq. (5b), the third phonon must have either $l''=0$ if it is an N process or $l''=n$ if it is a U process. Thus, the $(\pm 1,1)$ F phonons can undergo N decay into the $(l=0)$ L and T branches but not U decay, which can only occur into any of the six $l=n$ optic branches subject to the restrictions of Eqs. (5a) and (5c). In fact, consideration of all three-phonon processes allowed by Eq. (5b) shows that while three acoustic phonons can undergo N scattering, for umklapp scattering if l and l' correspond to acoustic modes, the only possible values of l'' are $l''=n$, $l''=n\pm 1$, and $l''=n\pm 2$. This means that for achiral nanotubes with $n\geq 4$, the l'' phonon cannot reside in an acoustic branch, and therefore, *U processes involving three acoustic phonons are not possible*. Calculations of the lattice thermal conductivity of bulk and nanostructured systems commonly include only the acoustic branches. The above considerations demonstrate that doing so in SWCNTs is conceptually incorrect.

Figure 1 illustrates the above points for the case of a (10,0) nanotube. It shows the lower portion of the phonon dispersions for $l=0$ (green lines), $l=\pm 1$ (blue lines), and $l=-9$ (red lines). The solid (dashed) lines correspond to phonon branches inside (outside) the first Brillouin zone. A lower-lying N process where two phonons from the degenerate (1,1) and $(-1,1)$ F branches decay into a (0,2) L branch phonon is indicated by the two thin black arrows. Also shown is a higher-lying U process in which (1,1) F and (0,1) T phonons decay into an out-of-zone mode in an $l''+l_G=1$ branch. Projection of this mode back into the first Brillouin zone using $l_G=n$ (horizontal black arrow) puts it in an $l''=-9$ branch. Also shown by the dashed arrows is an umklapp process involving only acoustic modes. This process satisfies Eqs. (5a) and (5c), but it cannot actually occur because it violates the l selection rule, Eq. (5b). Inclusion of such processes or others that do not satisfy the correct l selection rule would give incorrect contributions to the three-phonon scattering rates.

To describe phonon thermal transport, we consider a nanotube of length, L, connected at either end to reservoirs having a slight temperature difference. The resulting small temperature gradient, dT/dz, along the nanotube (z) axis creates a nonequilibrium phonon distribution, $n_\lambda=n_\lambda^0+n_\lambda^1$. The distribution, n_λ^1, results from the temperature gradient and is responsible for the thermal current. It can be obtained by solving the linearized phonon Boltzmann equation.[1,13,27,28] Because of its complexity, the solution of the phonon BTE is typically estimated using various phonon RTAs. However, the inelastic nature of the phonon-phonon scattering precludes, in principle, the use of an RTA.[1] Therefore, we have implemented an exact solution of the linearized phonon Boltzmann equation for the SWCNTs. The first such approach was implemented in Ref. 13, which examined the length dependence of the thermal conductivity of SWCNTs and demonstrated the importance of higher order anharmonicity in obtaining a convergent result in the diffusive limit, $L\rightarrow\infty$. Unlike that work, here we calculate the full three-phonon scattering rates from Eqs. (2) and (3) instead of using the LWA, we include all three-phonon scattering channels [*aaa*, *aao*, *aoo* and *ooo*, where $a(o)$ stands for acoustic (optic) phonon], and we use the l selection rule. We write the deviation from equilibrium $n_\lambda^1=-n_\lambda^0(n_\lambda^0+1)\beta F_\lambda dT/dz$, which allows us to cast the phonon Boltzmann equation as a set of coupled equations for the functions, F_λ,

$$F_\lambda = F_\lambda^0 + \Delta F_\lambda, \tag{6}$$

with

$$F_\lambda^0 = \frac{v_\lambda \hbar\omega_\lambda n_\lambda^0(n_\lambda^0+1)}{TQ_\lambda}, \tag{7}$$

$$Q_\lambda = \sum_{\lambda'\lambda''}\left[W^{(+)}_{\lambda\lambda'\lambda''} + \frac{1}{2}W^{(-)}_{\lambda\lambda'\lambda''}\right] + \frac{n_\lambda^0(n_\lambda^0+1)}{\tau_\lambda^b}, \tag{8}$$

$$\Delta F_\lambda = \frac{1}{Q_\lambda}\sum_{\lambda'\lambda''}\left[W^{(+)}_{\lambda\lambda'\lambda''}(F_{\lambda''}-F_{\lambda'}) + \frac{1}{2}W^{(-)}_{\lambda\lambda'\lambda''}(F_{\lambda''}+F_{\lambda'})\right]. \tag{9}$$

The presence of ΔF_λ reflects the inelastic nature of the three-phonon scattering, which couples out-of-equilibrium phonons in each mode λ to many others. If this term is neglected, a single-mode RTA results. The function, F_λ, is related to the scattering time, τ_λ in Eq. (1) as τ_λ

$=F_\lambda(T/v_\lambda\hbar\omega_\lambda)$. In Eq. (8), $\tau_\lambda^b=L/2|v_\lambda|$ is a boundary scattering time. For L much smaller than the anharmonic phonon mean free path, there is no three-phonon scattering so $F_\lambda=F_\lambda^0=v_\lambda\hbar\omega_\lambda\tau_\lambda^b/T$ and therefore $\tau_\lambda=\tau_\lambda^b$, which correctly reproduces the thermal conductivity in the ballistic limit, where $L\to 0$.[13,23] On the other hand, for L much larger than the phonon mean free path, the term containing τ_λ^b in Eq. (8) becomes negligible, which gives the diffusive limit.

The sums in Eqs. (8) and (9) are over the phase space of three-phonon processes with one phonon starting in mode λ. This phase space is calculated for both N and U processes and scattering between all combinations of acoustic and optic phonons that satisfy the selection rules, Eq. (5). Given a particular mode, λ, there are a large number of branches [e.g., $12n\times 12n$ for $(n,0)$ or (n,n) SWCNTs] to scan in search of corresponding pairs (λ',λ'') that satisfy energy and momentum conservation. Use of the l selection rule and exploitation of the many phonon branch degeneracies dramatically reduces this numerical bottleneck. Of the hundreds of thousands of different scattering events of type *aaa*, *aao*, *aoo*, and *ooo* that are obtained, we find that the *aao* channel most strongly suppresses the lattice thermal conductivity. Just *aaa* scattering alone does not provide thermal resistance, as described above; *aoo* scattering processes involving two optic phonons are far more numerous but typically much weaker than the *aao* processes because the higher-lying optic modes are less likely to be thermally excited.

III. RESULTS AND DISCUSSION

We calculate the thermal conductivity for each length SWCNT, L, by solving Eq. (6) using an iterative procedure.[13,27,28] To begin the iteration, we take $\Delta F_\lambda=0$ giving $F_\lambda=F_\lambda^0$ from Eq. (6) (single-mode RTA). Inputting these F_λ into Eq. (9) gives a new ΔF_λ and so a new F_λ. This process is repeated until the newly obtained F_λ are identical to those from the previous iteration. Upon each iteration, the τ_λ obtained from the F_λ are used in Eq. (1) to calculate the thermal conductivity.

We first explore the role of N and U processes on the thermal conductivity of a 10 μm SWCNT. Figure 2 shows the thermal conductivity calculated for a (10,0) SWCNT at room temperature (300 K) as a function of the number of iterations. The blue curve corresponds to the case where all N and U processes are included. The zeroth order (RTA) thermal conductivity for this case is $\kappa_0=1460$ W/m K. A converged thermal conductivity, $\kappa=2242$ W/m K, is rapidly achieved with iteration. That the converged value, κ, is significantly higher than κ_0 reflects the fact that the RTA provides a poor approximation to κ for SWCNTs of sufficient length that phonon-phonon scattering is important. The red curve shows the effect of turning off the umklapp scattering. The RTA value of $\kappa_0\approx 1600$ W/m K for this case is not much higher than the case where both N and U processes are included. However, with increasing iteration, κ increases dramatically, approaching the ballistic limit as it must when resistive scattering processes are removed. Here the solution of Eq. (6) in the limit, $L\to\infty$ is: $F_\lambda=\Delta F_\lambda$, which corresponds to a vanishing collision integral in the phonon BTE. In this

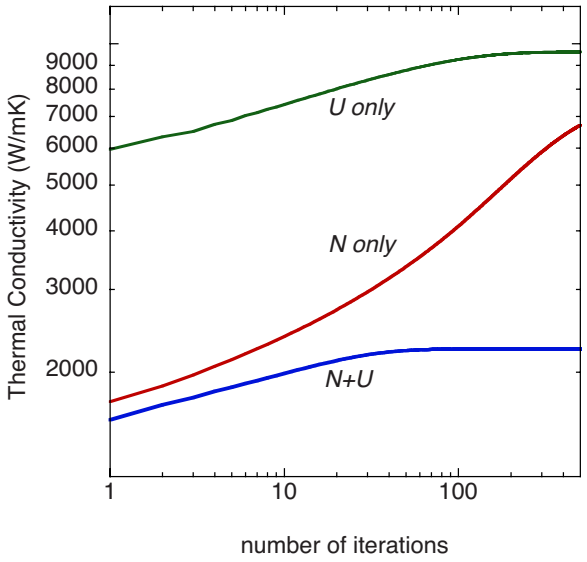

FIG. 2. (Color online) Intrinsic phonon thermal conductivity of a 10 μm (10,0) SWCNT as a function of number of iterations for the case where both N and U processes are included (blue curve), only N processes are included (red curve), only U processes are included (green curve).

hypothetical case, a flowing phonon distribution will not relax to equilibrium in the absence of a temperature gradient, and the thermal conductivity diverges. The green curve illustrates the behavior of κ when the N processes have been removed and only U processes are retained. For this case, significantly higher values of $\kappa_0\approx 6000$ W/m K and $\kappa\approx 9600$ W/m K are obtained. This occurs because of large contributions from the low frequency region of the integral in Eq. (1) where almost no U scattering processes occur. As a result, with only U scattering included, both κ and κ_0 diverge in the limit, $L\to\infty$. Figure 2 highlights the interplay between N and U processes in determining the thermal conductivity of SWCNTs. The U processes produce thermal resistance while the N processes, which cannot themselves provide thermal resistance, redistribute phonons to higher q where umklapp scattering can take place. Both N and U processes are required in a proper physical description of the lattice thermal conductivity.

Figure 3 shows the calculated room temperature thermal conductivity of (10,0) and (10,10) SWCNTs plotted as a function of their length, L. We focus first on the (10,0) nanotube. The black curve shows κ_0 while the red curve gives κ. For small L, κ and κ_0 are almost identical reflecting the ballistic limit. With increasing L, the two curves become more and more separated. This reflects the transition to diffusive behavior where the weak umklapp scattering makes the RTA a poor approximation to the solution of the phonon BTE. For L extending up to about a hundred micrometers, both curves increase monotonically suggestive of a divergent thermal conductivity with length.

For very large L, κ_0 plateaus. This plateau arises because in the diffusive limit, as $q\to 0$ the N scattering rates of the type $F+F\leftrightarrow L,T$(such as depicted in Fig. 1) become singular. This keeps the contributions from each acoustic branch finite. However, in the RTA, the N processes included in the

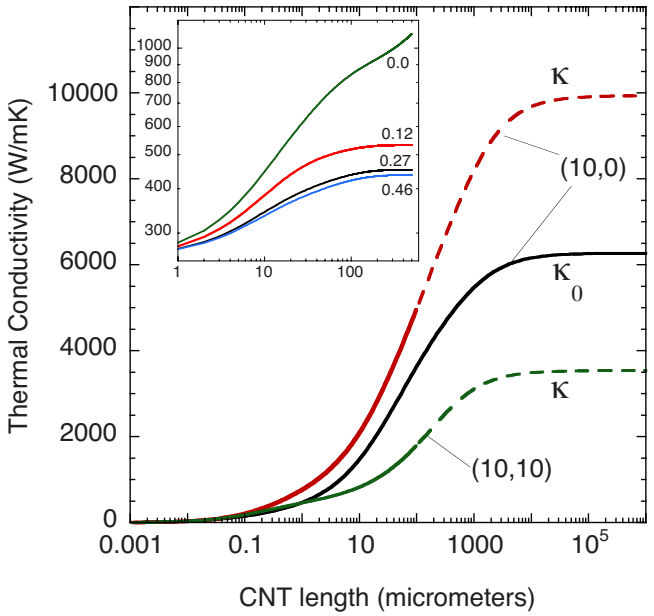

FIG. 3. (Color online) Intrinsic phonon thermal conductivity of (10,0) and (10,10) SWCNTs.vs. length. κ_0 gives the RTA (zeroth order) thermal conductivity (solid black curve), while κ is the iterated thermal conductivity [red curve—(10,0), green curve—(10,10)]. The dashing shows the estimated effect of including higher order terms in the anharmonic expansion of the interatomic potential. Inset shows the F branch contribution to κ vs iteration for different cutoff frequencies, as described in the text.

scattering rates are not properly represented because they enter in a purely resistive fashion. We find that beyond ~ 100 μm, the iterated thermal conductivity in fact does not converge reflecting a divergence in the F mode contribution to κ. Here, with increasing iteration the F branch nonequilibrium distribution function grows without bound for small q. The divergence in the scattering $F+F \leftrightarrow L,T$ rates for $q \rightarrow 0$ suggests that higher order phonon-phonon scattering is important. We have estimated the possible suppressive effects of higher order scattering on the small q flexure modes by introducing a small cutoff frequency, ν_c, below which the flexure mode functions, $F_\lambda = F_{\pm 1,1}(q)$, upon each iteration are fixed to their zeroth order value. In this case, we obtain the dashed red curve in Fig. 3 with a plateaued value of $\kappa \approx 9800$ W/m K. We note that inclusion of higher order anharmonicity was also required in Ref. 13 in order to achieve a plateaued result. The inset shows the effect of imposing this restriction. The curves show the F mode contribution to κ as a function of the number of iterations for different values of ν_c, indicated by the numbers above each curve. For $\nu_c = 0.0$ THz, the F mode contribution diverges, while for very small $\nu_c = 0.12$ THz, it drops in value and immediately converges with iteration. For slightly larger values of ν_c, successive F mode contributions begin to coincide. We note that the largest value considered is more than an order of magnitude smaller than the zone boundary F mode frequency of $\nu \sim 10$ THz. Even with this, the κ obtained from the full solution of the phonon Boltzmann equation is considerably larger than the RTA value of $\kappa \approx 6200$ W/m K. That this is the case is a consequence of the very small phase space for umklapp scattering in SWCNTs and other carbon-based materials.

The green curve shows κ for the (10,10) SWCNT, using the cutoff scheme for the F branch contributions to κ described above. The decrease in κ for the (10,10) nanotube is partly due to the increased cross-sectional area in Eq. (1), which reduces κ by $\sqrt{3}$ compared to the (10,0) case. An additional decrease of roughly the same amount occurs because with increasing radius the optic branch frequencies are lower, which enhances the acoustic-optic phonon scattering.

We now comment on the commonly used LWA for three-phonon scattering rates. In this approximation, the three-phonon matrix element in Eqs. (2) and (3) is taken to behave as[10–13,15] $|\Phi_{\lambda\lambda'\lambda''}|^2 \sim (qq'q'')^2 \sim (\omega\omega'\omega'')^2$. Implicit in this form are the assumptions that (a) q, q', and q'' are all small, and (b) the long-wavelength acoustic phonon dispersions are linear: $\omega \propto q$. We note that condition (a) is in principle incompatible with U scattering since at least one of the phonons must have large wave vector. Therefore, one might expect the LWA to be more appropriate for N scattering. For the N scattering case, the replacement $qq'q'' \sim \omega\omega'\omega''$ for linear acoustic phonon branches is valid. For three-phonon scattering involving at least one phonon from a quadratic branch, such as occurs in SWCNTs, graphene and graphite, the above replacement is no longer correct. For example, for the N process shown in Fig. 1, which involves two F modes, $|\Phi_{\lambda\lambda'\lambda''}|^2 \sim (qq'q'')^2 \sim \omega\omega'\omega''^2 \neq (\omega\omega'\omega'')^2$. We have carefully examined the behavior of the three phonon matrix element $\Phi_{\lambda\lambda'\lambda''}$ in the limit where q, q', and q'' are all small by expanding the linear and quadratic acoustic mode eigenvectors in Eqs. (3) and (4) in powers of q: $e^\lambda_\alpha(\ell\kappa) = \Sigma_i a^\lambda_{i\alpha}(\ell\kappa) q^i$. The coefficients, $a^\lambda_{i\alpha}(\ell\kappa)$, are determined to third order in q using a perturbation approach.[29] We have found that the $|\Phi_{\lambda\lambda'\lambda''}|^2 \sim (qq'q'')^2$ dependence holds for both linear and quadratic acoustic phonon branches but $|\Phi_{\lambda\lambda'\lambda''}|^2 \sim (\omega\omega'\omega'')^2$ does not hold when quadratic branches are included. Interestingly, use of a model central potential for the third order IFCs (Ref. 13) yielded $|\Phi_{\lambda\lambda'\lambda''}|^2 \sim (\omega\omega'\omega'')^2$ even with quadratic modes included. This is likely due to the lack of bond bending terms in the central potential model. These bond bending terms are incorporated in the Tersoff potential used in the present work.

In comparing to our calculated results for both (10,0) and (10,10) SWCNTs, we find that the RTA used with the LWA gives results that are in poor agreement with our full calculations. Figure 4 illustrates the behavior for a (10,10) nanotube as a function of its length. The black and green curves give κ_0 and κ for the full calculation, while the dotted (dashed) red curve gives the LWA results with both N and U processes (just U processes) included. For $L \sim 1$ μm, the LWA curves sandwich the full RTA result. For large L, the LWA with only U processes diverges and the LWA with U and N processes saturates to a value more than ten times larger than the full calculation.

In this work, we used a cross-sectional area, of $A = \pi d \delta$ so that $A \propto d$. This choice was made so that we could directly compare our calculated thermal conductivities with available experimental results.[5,6] An alternative estimate often found in the literature is $A = \pi d^2/4$, giving a scaling $A \propto d^2$. Since the thermal conductivity, κ, is inversely proportional to A, had

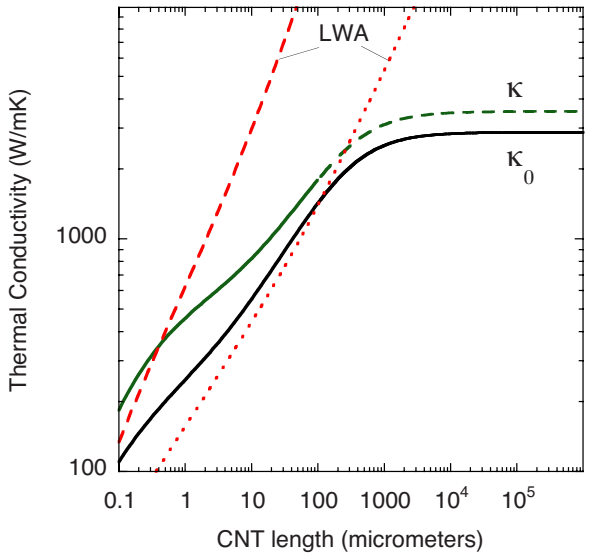

FIG. 4. (Color online) Intrinsic phonon thermal conductivity of (10,10) SWCNT vs length. Black and green curves give κ_0 and κ; red curves show the LWA including N and U processes (dotted) and just U processes (dashed).

we used this alternative estimate, all thermal conductivities would be rescaled by $4\delta/d$. Thus, for nanotube diameters smaller (larger) than 4δ, the thermal conductivity would be increased (decreased). For example, for the (10,0) SWCNT, the calculated thermal conductivity would increase by 60%, while that of the (10,10) SWCNT would be roughly unchanged.

Quantitative consideration of the chirality dependence and fourth-order phonon-phonon scattering is beyond the scope of the present work. Nevertheless, we consider here the qualitative differences between achiral and chiral SWCNTs based on their different symmetries. In chiral tubes the horizontal and vertical reflection symmetries are removed. This results in a lifting of the double degeneracy of many phonon branches. The form of the azimuthal selection rule for three-phonon umklapp scattering in chiral tubes is somewhat more complex than expressed in Eq. (5b).[25,26] However, we have verified that the phonon-phonon umklapp scattering l selection rules for both achiral and chiral nanotubes up through fourth order obey the requirement demonstrated here that umklapp scattering processes must involve at least one optic mode. Thus, this constraint is a general property for all SWCNTs.

The calculations performed here were for defect free SWCNTs. In real SWCNTs defects are present that lower the thermal conductivity. Unlike the anharmonic phonon-phonon scattering, treatment of defects can be incorporated straightforwardly into the present Boltzmann transport approach using a relaxation time to represent the defect scattering. This is because the defect scattering is an elastic process while the phonon-phonon scattering is not. As an example, we have estimated the effect of the presence of 1% C^{13} isotopic impurities in C^{12}. This concentration is roughly that found in type IIa naturally occurring diamond.[3,4] The isotopic impurity scattering rate is[28] $W^{imp}_{\lambda\lambda'}=\frac{\pi}{2}g_2\omega_\lambda\omega_{\lambda'}n^0_\lambda(n^0_{\lambda'}+1)\Sigma_\kappa|\hat{e}^{\lambda *}_\kappa\cdot\hat{e}^{\lambda'}_\kappa|^2\delta(\omega_{\lambda'}-\omega_\lambda)$, which can be incorporated directly into Eq. (8). Here g_2 is the mass variance parameter,[30] which describes the concentration and mass change for each isotope type. We find that for a (10,10) 3 μm nanotube the thermal conductivity decreases $\sim$25% at room temperature. This large effect is qualitatively consistent with that found in diamond[3,4] and with previous theoretical investigations.[31]

Experimental measurements of the lattice thermal conductivity of SWCNTs having lengths $L\sim 3$ μm have been performed,[5,6] and yield room temperature values of $\kappa \approx 3000-3500$ W/m K. These values are much higher than our corresponding calculated results of 1350 and 600 W/m K for (10,0) and (10,10) SWCNTs, respectively. One possible reason for this difference is the fact that the anharmonicity of the Tersoff empirical potential for carbon is too strong. We have corroborated this qualitatively by examining bulk diamond using the Tersoff IFCs, where we find that the calculated room temperature thermal conductivity is about 40% below the measured value. In fact, κ is quite sensitive to the strength of the anharmonic IFCs since these are squared in the three-phonon scattering rates entering Eq. (2). We have also generated IFCs using the Brenner interatomic potential[32] but found comparably low thermal conductivities using it. In some sense, the difference between our theoretical results and experiment is not surprising as these potentials have been optimized to fit structural data, not phonon spectra and thermal conductivity. And, it is important to point out that there are no adjustable parameters in our model.

IV. SUMMARY AND CONCLUSIONS

In summary, an efficient scheme has been presented here to calculate the intrinsic phonon thermal conductivity of SWCNTs. This approach allows consideration of a wide range of diameters and chiralities. Exploiting the azimuthal symmetry in calculating phonon frequencies combined with use of the l selection rule allow rapid evaluation of the three-phonon scattering rates and make tractable the solution of the full phonon BTE for SWCNTs including all acoustic and optic branches. We have demonstrated that the commonly used relaxation time approximation and long-wavelength approximation give poor representations of the three-phonon scattering rates and thermal conductivity in SWCNTs. We have shown that inclusion of both N and U phonon-phonon scattering processes, and of the acoustic-optic phonon scattering channels is essential in order to properly describe the thermal conductivity of SWCNTs.

ACKNOWLEDGMENTS

The authors gratefully acknowledge the National Science Foundation and the Donors of the American Chemical Society Petroleum Research Fund for support of this research. N.M. acknowledges support from ANR through project ACCATONE.

[1] J. Ziman, *Electrons and Phonons* (Oxford University Press, Oxford, 1960).
[2] L. Lindsay and D. A. Broido, J. Phys.: Condens. Matter **20**, 165209 (2008).
[3] L. Wei, P. K. Kuo, R. L. Thomas, T. R. Anthony, and W. F. Banholzer, Phys. Rev. Lett. **70**, 3764 (1993).
[4] D. G. Onn, A. Witek, Y. Z. Qiu, T. R. Anthony, and W. F. Banholtzer, Phys. Rev. Lett. **68**, 2806 (1992).
[5] C. Yu, L. Shi, Z. Yao, D. Li, and A. Majumdar, Nano Lett. **5**, 1842 (2005).
[6] E. Pop, D. Mann, Q. Wang, K. Goodson, and H. Dai, Nano Lett. **6**, 96 (2006).
[7] A. A. Balandin, S. Ghosh, W. Bao, I. Calizo, D. Teweldebrhan, F. Miao, and C. Ning Lau, Nano Lett. **8**, 902 (2008).
[8] J. Lukes and H. Zhong, ASME J. Heat Transfer **129**, 705 (2007) and references therein.
[9] D. Donadio and G. Galli, Phys. Rev. Lett. **99**, 255502 (2007).
[10] J. X. Cao, X. H. Yan, Y. Xiao, and J. W. Ding, Phys. Rev. B **69**, 073407 (2004).
[11] J. Wang and J.-S. Wang, Appl. Phys. Lett. **88**, 111909 (2006).
[12] Y. Gu and Y. Chen, Phys. Rev. B **76**, 134110 (2007).
[13] N. Mingo and D. A. Broido, Nano Lett. **5**, 1221 (2005).
[14] G. D. Mahan and Gun Sang Jeon, Phys. Rev. B **70**, 075405 (2004).
[15] P. G. Klemens, Solid State Phys. **7**, 1 (1958).
[16] C. T. White, D. H. Robertson, and J. W. Mintmire, Phys. Rev. B **47**, 5485 (1993).
[17] R. A. Jishi, M. S. Dresselhaus, and G. Dresselhaus, Phys. Rev. B **47**, 16671 (1993).
[18] N. Hamada, S.-I. Sawada, and A. Oshiama, Phys. Rev. Lett. **68**, 1579 (1992).
[19] R. Saito, M. Fujita, G. Dresselhaus, and M. S. Dresselhaus, Phys. Rev. B **46**, 1804 (1992).
[20] V. N. Popov, V. E. Van Doren, and M. Balkanski, Phys. Rev. B **61**, 3078 (2000).
[21] J. Tersoff, Phys. Rev. Lett. **61**, 2879 (1988).
[22] G. Leibfried and W. Ludwig, Solid State Phys. **12**, 275 (1961).
[23] N. Mingo and D. A. Broido, Phys. Rev. Lett. **95**, 096105 (2005).
[24] There has been considerable discussion about this choice (see Ref. 8). We employ it here to better connect with previous work.
[25] S. Reich, C. Thomsen, and J. Maultzsch, *Carbon Nanotubes: Basic Concepts and Physical Properties* (Wiley-VCH, Weinheim, Germany, 2004).
[26] N. Bozovic, I. Bozovic, and M. Damnjanovic, J. Phys. A **18**, 923 (1985).
[27] M. Omini and A. Sparavigna, Nuovo Cimento D **19**, 1537 (1997).
[28] D. A. Broido, A. Ward, and N. Mingo, Phys. Rev. B **72**, 014308 (2005).
[29] M. Born and K. Huang, *Dynamical Theory of the Crystal Lattices* (Oxford University Press, Oxford, 1954).
[30] M. Asen-Palmer, K. Bartkowski, E. Gmelin, M. Cardona, A. P. Zhernov, A. V. Inyushkin, A. Taldenkov, V. I. Ozhogin, K. M. Itoh, and E. E. Haller, Phys. Rev. B **56**, 9431 (1997).
[31] I. Savić, N. Mingo, and D. A. Stewart, Phys. Rev. Lett. **101**, 165502 (2008).
[32] D. W. Brenner, O. A. Shenderova, J. A. Harrison, S. J. Stuart, B. Ni, and S. B. Sinnott, J. Phys.: Condens. Matter **14**, 783 (2002).